



Numerical study of atmospheric ice accretion on rotating geometric cross sections with fins

Umair N Mughal and Muhammad S Virk

Abstract

This paper describes the numerical study of atmospheric ice accretion on rotating geometric cross sections, *circular, hexagon and square*, all having fins, to select an optimum geometric cross section for use as a rotating part of a newly-proposed designed icing sensor. Computational fluid dynamics-based numerical analyses were carried out in this research work to understand and analyse the atmospheric ice growth on these rotating cross sections at varying operating and geometric parameters. A comparison of accreted ice profile shapes from numerical analysis was also made with the experiments, carried out at cryospheric environment simulator (CES), Shinjo Japan. A good agreement was found between numerical and experimental results.

Keywords

Atmospheric ice, geometric cross sections, rotating, fins, ice growth

Date received: 30 August 2015; accepted: 2 February 2016

Introduction

Human activities in cold regions are increasingly extending, where atmospheric icing is a potential hazard which can affect human activities especially in the construction, energy, maritime and aviation-related sectors. Various structures in cold regions have been reported to damage or destroy on numerous occasions due to the added mass of accreted ice or an increase in aerodynamic interaction due to icing, leading to unacceptable dynamic movements.¹ Therefore, better knowledge of frequency and duration of icing events as well as maximum ice loads is a crucial parameter for the safe structural design and operation in cold regions.

Atmospheric icing is the term used to describe the ice accretion on structures, which occurs when freezing rain drops, and snow particles or super cooled water droplets come into contact with the exposed structural surface.² Atmospheric ice can be classified as: *rime, glaze or mixed ice*,³ depending upon variation in density. Two processes mainly govern intensity of ice accretion on any structure: the impingement of super cooled water droplets and surface thermodynamics, which determines which portion of the impinging water freezes or on other hand melts the previously accreted ice. Most investigations related to ice accretion

on structures have been performed using either ordinary wind tunnel with artificial ice templates attached to profile or icing wind tunnel, but for the last three decades or so computational fluid dynamics (CFD)-based numerical techniques have begun to play a significant role in understanding and simulating the ice growth on various structures.

Numerical study of atmospheric ice accretion on structures includes the computation of mass flux of icing particles as well as determination of the icing conditions.⁴ This can be numerically simulated by means of integrated thermo-fluid dynamic models, which requires the use of multiphase analysis in order to obtain the aerodynamics flow field, the droplet behaviour, surface thermodynamics and phase change. Most developments in the numerical modelling of ice accretion have focused on aerospace sector and very few improvements have been reported in the research field

Arctic Technology Research Team, Institute of Industrial Technology, University of Tromsø, Norway

Corresponding author:

Umair N Mughal, Arctic Technology Research Team, Institute of Industrial Technology, University of Tromsø, Norway.
Email: umair.n.mughal@uit.no



of ground structural icing. Various numerical studies related to the atmospheric icing on structures can be found in the literature. The first attempts were made from the late 1970s, where researchers such as Ackley and Templeton,⁵ Lozowski et al.,⁶⁻⁸ McComber et al.,^{9,10} and Smith and Barker¹¹ concentrated on understanding the physical ice accretion processes and developing numerical models to predict the severity of icing on structures. Later Makkonen,^{12,13} Finstad et al.,¹⁴ Shin et al.,^{15,17} Boutanios, 1 Skelton et al.¹⁸ and Virk et al.¹⁹⁻²¹ worked on numerical modelling of the atmospheric ice accretion on different structures.

This paper describes the numerical study of atmospheric ice accretion on three different rotating geometric cross sections having fins: *circular*, *hexagon* and *square*. The parametric analysis are carried out by considering different operating and geometric conditions to get a better understating of ice accretion physics on each geometric cross section. The optimum geometric cross section, selected from this parametric study, is meant to be used as a rotating part of a newly proposed designed icing sensor of NUC. Figure 1 shows the computer-aided design (CAD) model of the proposed design of icing sensor with three different rotating cross sections on top (circular, square and hexagon).

Numerical approach

Computational fluid dynamics-based numerical modeling of atmospheric ice accretion on structures mainly involves the airflow behaviour, droplet impingement and surface thermodynamics. First, it requires the airflow simulations; then super cooled water droplet behaviour is simulated to obtain the distribution of water impingement along the surface; and finally the surface thermodynamic analysis is performed to

estimate the ice growth. In this research work, the numerical analysis was carried out using computational fluid dynamics-based multiphase numerical solvers, FENSAP-ICE from NTI²² and ANSYS-FLUENT. Here, FENSAP-ICE was mainly used to simulate the airflow, droplet behaviour and resultant ice accretion, whereas ANSYS-FLUENT was used only in some cases to simulate the airflow behaviour of complex shapes, where complex turbulent behaviour is observed around the structure. In such cases, the results from ANSYS-FLUENT were coupled with the FENSAP for simulation of droplet behaviour and resultant ice accretion. Figure 2 shows the schematic overview of coupling of different processes used in these numerical simulations.

Airflow behaviour is numerically simulated by solving partial differential equations for the conservation of mass, momentum and energy. Spatial discretisation was carried out by Galerkin finite element method (FEM) and the equations were linearised by a Newton method.

$$\begin{aligned} \frac{\partial \rho_a}{\partial t} + \vec{\nabla} \cdot (\rho_a \vec{V}_a) &= 0 \\ \frac{\partial \rho_a \vec{V}_a}{\partial t} + \vec{\nabla} \cdot (\rho_a \vec{V}_a \vec{V}_a) &= \vec{\nabla} \cdot \sigma^{ij} + \rho_a \vec{g} \\ \frac{\partial \rho_a E_a}{\partial t} + \vec{\nabla} \cdot (\rho_a \vec{V}_a H_a) &= \vec{\nabla} \cdot (k_a (\vec{\nabla} T_a) + v_i \tau^{ij}) \\ &+ \rho_a \vec{g} \cdot \vec{V}_a \end{aligned} \quad (1)$$

where σ^{ij} is the stress tensor, k is the thermal conductivity, E is the internal energy and H is the enthalpy. The one equation Spalart Allmaras turbulence model was used as a compromise between acceptable computational cost and the required accuracy in simulating

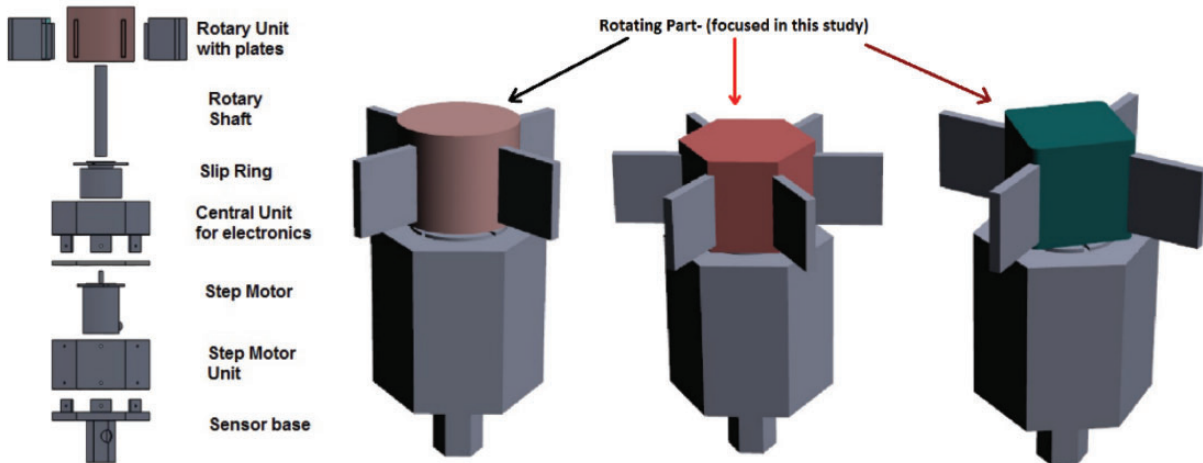


Figure 1. Computer-aided design of proposed icing sensor, with configuration of three different rotating cross sections.

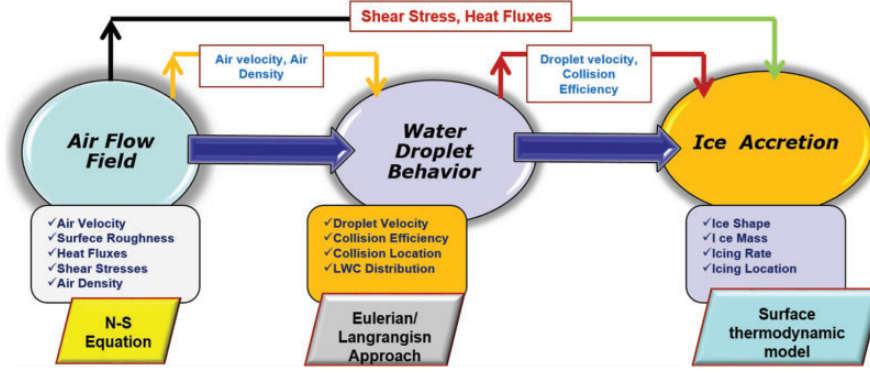


Figure 2. Schematic view of coupling of different processes involved in the numerical simulations.

the turbulent flow. Two-phase flow (air and water) was numerically simulated using Eulerian–Eulerian approach, where super cooled water droplets were assumed to be monodispersed and spherical. The Eulerian two-phase fluid model used, consists of the Navier–Stokes equation, augmented by the water droplets continuity and momentum equation. The water droplet drag coefficient is based on the empirical correlation for the flow around the spherical droplets described by Clift et al.²³

$$\begin{aligned} \frac{\partial \alpha}{\partial t} + \vec{\nabla} \cdot (\alpha \vec{V}_d) &= 0 \\ \frac{\partial (\alpha \vec{V}_d)}{\partial t} + \vec{\nabla} \cdot (\alpha \vec{V}_d \cdot \vec{V}_d) &= \frac{C_D Re_d}{24K} \alpha (\vec{V}_a - \vec{V}_d) + \alpha \left(1 - \frac{\rho_a}{\rho_d}\right) \frac{1}{Fr^2} \vec{g} \quad (2) \\ K &= \frac{\rho_d d^2 v_{a,\alpha}}{18 L_\alpha U_a}, \quad Fr = \frac{v_{a,\alpha}}{\sqrt{L_\alpha g}} \\ Re_d &= \frac{\rho_d d v_{a,\alpha} \|v_a - v_d\|}{\mu_a} \end{aligned}$$

where α is the water volume fraction, V_d is the droplet velocity, C_D is the droplet drag coefficient and Fr is the Froude number. Droplet collection efficiency on the surface is calculated using¹⁶

$$\beta = -\alpha u \cdot n \quad (3)$$

where n is the surface normal. The water flux at the surface is calculated by

$$m_w = LWC \cdot U_\infty \cdot \beta \quad (4)$$

On structural surface, the contamination caused by the impinging water droplets is modelled as thin liquid film, which may run back, forced by the shear stresses created by the airflow. Based on the surface thermodynamic conditions, part of the film may freeze,

evaporate or sublimate. Surface thermodynamic and icing rate are calculated by using the mass and energy conservation equations, considering the heat fluxes due to convective cooling, evaporative cooling, heat of fusion, viscous heating and kinetic heating.²⁴

$$\rho_f \left[\frac{\partial h_f}{\partial t} + \nabla \cdot (V_f h_f) \right] = V_\infty \cdot LWC \beta - m_{\text{evap}}^o - m_{\text{ice}}^o$$

$$Q_{in}^o = Q_{out}^o$$

$$Q_{\text{latent heat}} + Q_{\text{aerodynamic heat}} + Q_{\text{KE heat}} = Q_{\text{sublimative heat}} + Q_{\text{convective heat}} + Q_{\text{droplet, cooling heat}}$$

$$Q_{\text{aerodynamic, heating}} = \frac{r h_c v_\alpha^2}{2 C_p}$$

r = Adiabatic recovery factor,

$$(r = P_r^{1/2} \text{ for laminar and } r = P_r^{1/3} \text{ for turbulent flow})$$

$$P_r = 0.72$$

C_p = Specific heat of air, 1006 J/kgK

$$Q_{\text{latent, heat}} = (LWC \cdot \beta \cdot v_\alpha) \cdot [L_f + C_i (T_{\text{air}} - T_{\text{surface}})]$$

C_i = Specific heat of ice

L_f = Latent heat of fusion

$$Q_{\text{droplet, kinetic, energy}} = (LWC \cdot \beta \cdot v_\alpha) \frac{v_\alpha^2}{2}$$

$$Q_{\text{convection}} = h_c (T_{\text{surface}} - T_{\text{air}})$$

$$Q_{\text{sublimation}} = \chi_s e_o (T_{\text{surface}} - T_{\text{air}})$$

$$\chi_s = \frac{0.622 h_c L_s}{C_p P_t L_e^{0.66}}$$

$$e_o = 27.03$$

L_s = Latent heat of sublimation.

L_e = Lewis number, $1/P_r$

P_t = Total pressure of air

$$Q_{\text{droplet, cooling}} = \rho_a \beta v_\alpha C_{p,w} (T_{\text{surface}} - T_{\text{air}})$$

$$C_{p,w} = \text{Specific heat of water, } 4218 \text{ J/kgK} \quad (5)$$

Table 1. Operating conditions used for the simulations.

Free stream wind velocity (m/s)	10
Droplet size, MVD (μm)	35
Liquid water content (g/m^3)	0.5
Droplet distribution spectrum	Monodispersed
Rotational speed (r/min)	6
Atmospheric air temperature ($^{\circ}\text{C}$)	-10
Simulation time (minutes)	120
Cylinder diameter (mm)	162
Hexagon side length (mm)	162
Square side length (mm)	162
Fin length (mm)	94

Ice density was analytically calculated by using the Jones formula, defined as

$$R_M = -\frac{d \cdot \|\vec{V}_d\|}{2T_{\text{wall}}} \quad (6)$$

$$\rho_{\text{ice}} = \begin{cases} 0.21R_M^{0.53} & R_M \leq 10 \\ R_M/(1.15R_M + 2.94) & 10 \leq R_M \leq 60 \\ 0.84 & R_M \geq 60 \end{cases}$$

ALE (*Arbitrary Lagrangian Eulerian*) formulation was used in FENSAP-ICE for the mesh displacement due to ice accretion in time. This approach adds the grid speed terms to the Navier–Stokes equations to account for the mesh velocity.²⁵ Structured grid was used and mesh sensitivity analysis was carried out to accurately determine the boundary layer characteristics (*shear stresses and heat fluxes*). $Y+$ value less than 1 was used near the wall to better estimate the shear stresses. The initial sand grain roughness height for the surface was assumed to be 0.5 mm and also a variable surface roughness model of FENSAP-ICE based on the beads was used.²⁶ The two-phase flow was solved using Eulerian–Eulerian approach in FENSAP-ICE. The main advantage of using Eulerian–Eulerian approach is that the same mesh can be used for multiphase flow calculations and ice geometry. Rotational effects were introduced by applying a tangential velocity on the rotating surface grid nodes. By describing the rate of rotation (r/min), the components of tangential velocity are computed for each surface node depending on its normal distance from the axis of rotation. The numerical simulations were carried out at the operating and geometric conditions specified in Table 1.

Results and discussion

The focus of this numerical study has been on understanding the ice growth on three different rotating

geometric cross sections with fins, so that an optimum geometric cross section can be selected for rotating component of the newly-designed icing sensor the Atmospheric Icing Research Team. Parametric numerical analysis was carried out at different operating and geometric conditions to better understand the phenomena. The results obtained from numerical simulations (ice profile shape) of circular and hexagonal cross sections were also compared with the experimental results, obtained from experimental expedition of atmospheric icing research team conducted at cryospheric environment simulator (CES) Japan.

Study of geometric parameters variation

Effects of geometric shape. To study the effects of geometric shape variations on ice accretion, analysis was carried out at a wind speed of 10 m/s, MVD = 35 μm and $T = -10^{\circ}\text{C}$ for both rotating and non-rotating conditions. Figure 3 shows the velocity streamlines across each geometric cross section. Results show a more streamlined airflow behaviour around circular cross section, compared with hexagon and square, particularly between fins. Stronger recirculating flow zone is observed in the case of hexagon and square cross section compared with circular cross section, which adversely can affect the droplet behaviour and heat fluxes involved in resultant surface thermodynamic.

Figure 4 shows the droplet collision efficiency for each geometric cross section. The results show a smooth distribution of droplet impingement on circular cross section as compared to hexagon and square. In case of hexagon, impingement of water droplets is irregular and accumulation of run backwater is observed near the fin root section. In case of square, droplets are also irregularly colliding along the fin surface, where as in case of circle a smooth distribution of droplet impingement is observed both along the fins and the cylindrical cross section surface. The airflow and droplet behaviour are coupled with each other and any significant change in the airflow behaviour affects the resultant droplet impingement distribution and ice accretion.

Figure 5 shows the resultant accreted ice profiles on each geometric cross section for both rotating and non-rotating conditions. The analysis shows a better distribution of ice accretion along the geometric surface in the case of rotation, compared with the non-rotating case. This is mainly because, in the case of rotation, the droplet impingement along the surface area is smoothly distributed, compared with the non-rotational case, where the droplets mainly collide with the surface area along the windward side. Such smooth distribution of ice in the case of rotation can help to minimise the dynamic instabilities due to fluid–structure interaction, while ice accretes on any structure.

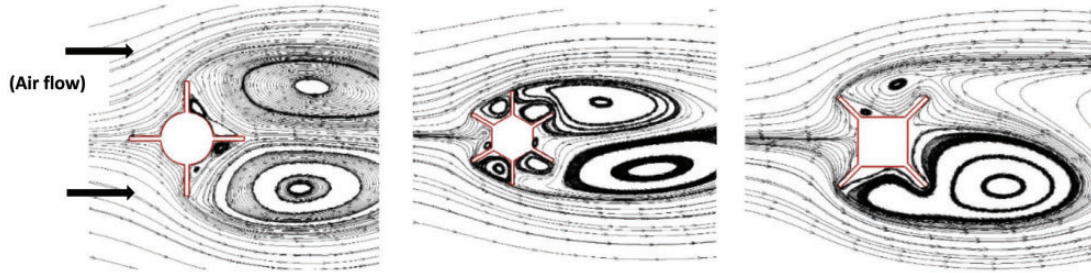


Figure 3. Velocity streamlines across different cross sections.

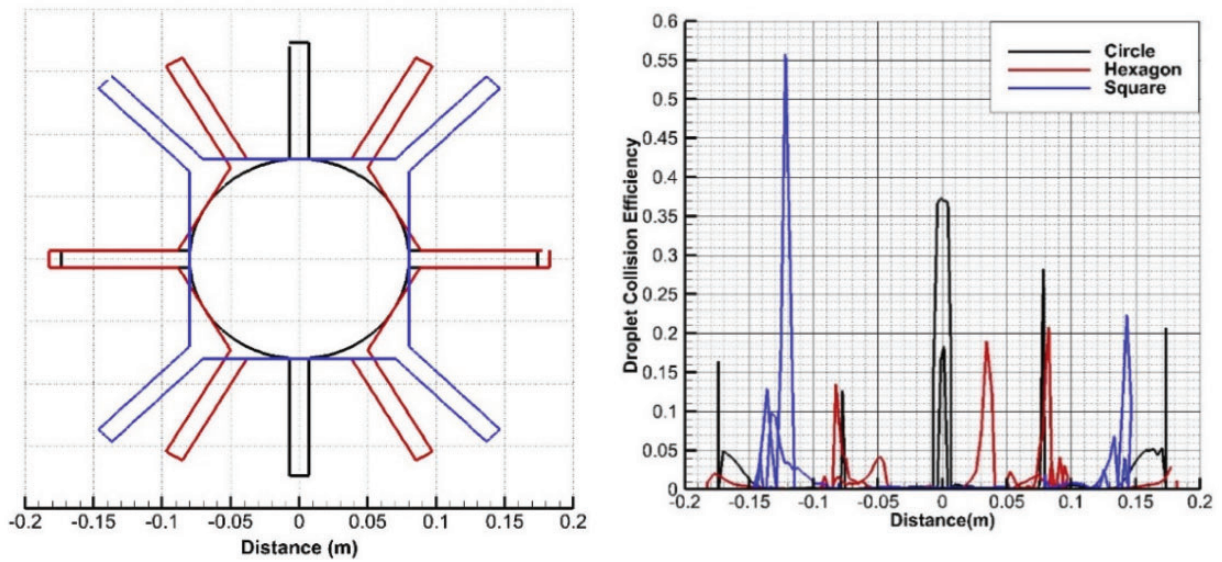


Figure 4. Droplet collision efficiency along rotating geometric cross section, $v = 10 \text{ m/s}$, $MVD = 35 \mu\text{m}$.

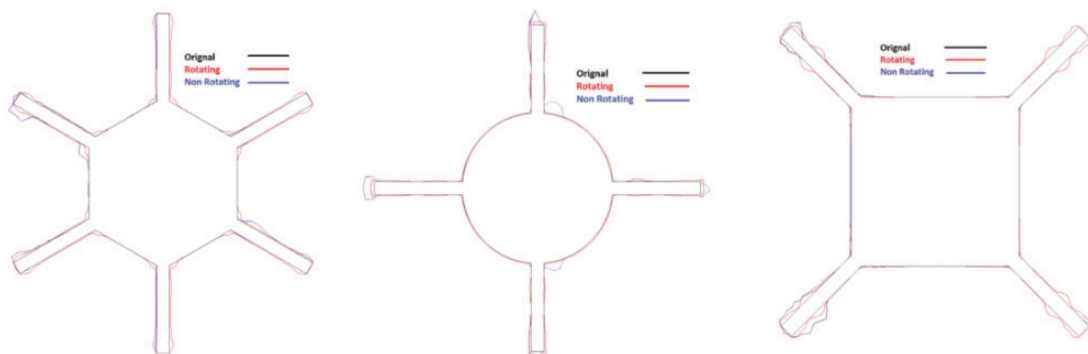


Figure 5. Ice accretion along each geometric cross section, $t = 120 \text{ min}$.

For rotating cross sections, at $r/\text{min} = 6$, ice accretion along the circular geometry is found to be more smooth and evenly distributed compared with hexagon and square cross sections. The process of ice accretion along any structure is generally coupled with the air-flow and droplet behaviour around that structure. That

is also found in this case study. Irregular ice shapes were observed along fins in case of square and hexagon cross sections due to more complex air and droplet flow behaviour between fins.

To get a better overview, further analysis was carried out to calculate the accreted ice growth and thickness

for each cross section. Figure 6 shows the ice growth and thickness distribution along each cross section and the results clearly highlight the uneven distribution of ice loads along the hexagon and square cross sections. Especially in the case of square cross section, the ice load distribution is more uneven along the fins, whereas in case of hexagon cross section, more water run back along the fins is observed, which leads to accumulation of more ice near the fin root section.

To further analyse the ice growth, numerical analysis on circular and hexagonal cross sections was extended for a total simulation time of 5 h (300 min). Figure 7 shows that ice load distribution along circular cross section stays smooth even for longer intervals of time, whereas in the case of hexagon cross section the

accumulated ice shapes become more irregular for longer durations of time.

The numerically simulated ice growth on circular and hexagonal shapes were also compared with the experiments carried out at cryospheric environment simulator (CES) Shinjo, Japan. Data for the droplet size and liquid water content during experiments were not available at CES, therefore exact comparison of ice load and thickness was not possible and only the accreted ice shapes were compared with each other. Overall, the accreted ice shapes on circular and hexagonal cross sections using numerical simulation were found to be in reasonably good agreement with the experimental results. Figure 8 shows the accreted ice shapes on circular and hexagonal cross section for

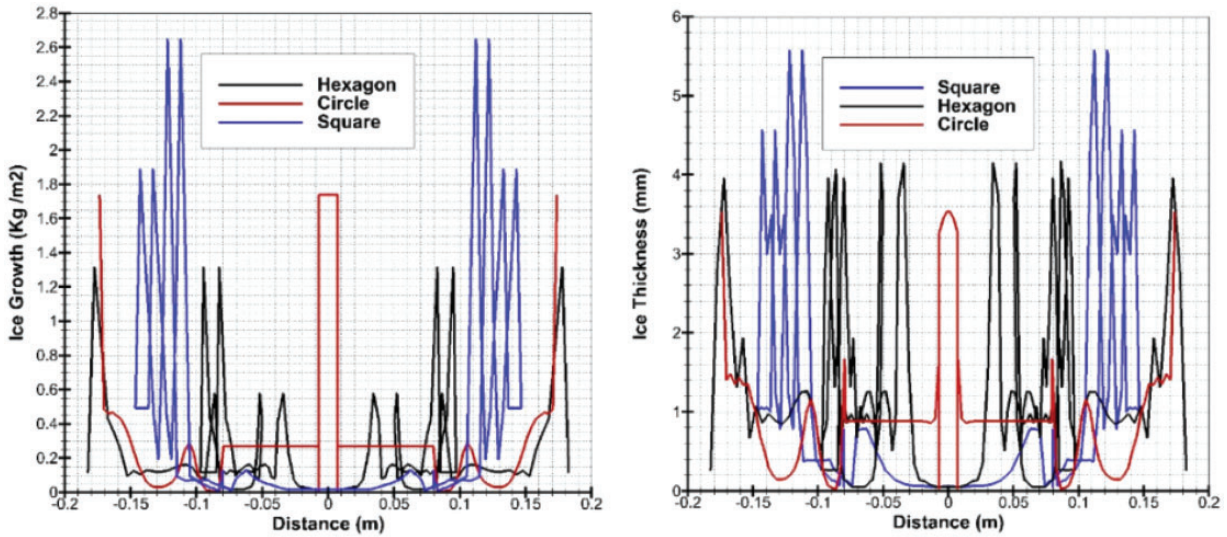


Figure 6. Ice growth and thickness distribution along each rotating geometric cross section for $t = 120$ min.

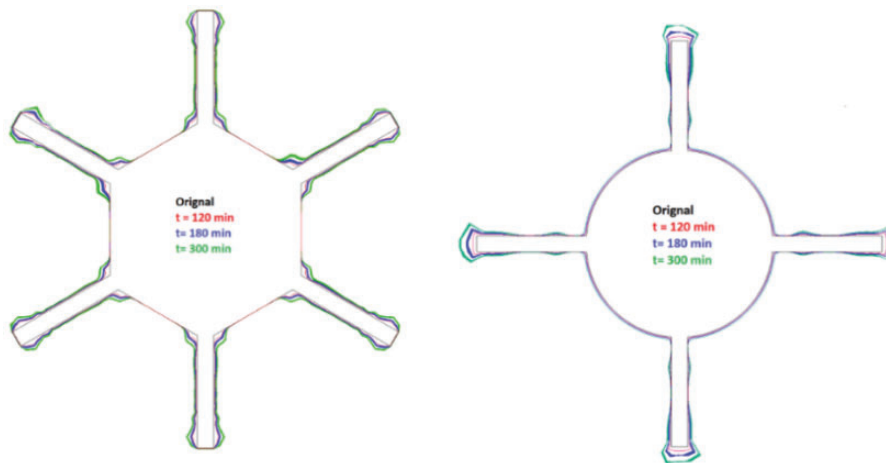


Figure 7. Ice accretion on circular and hexagonal cross sections for different time intervals.

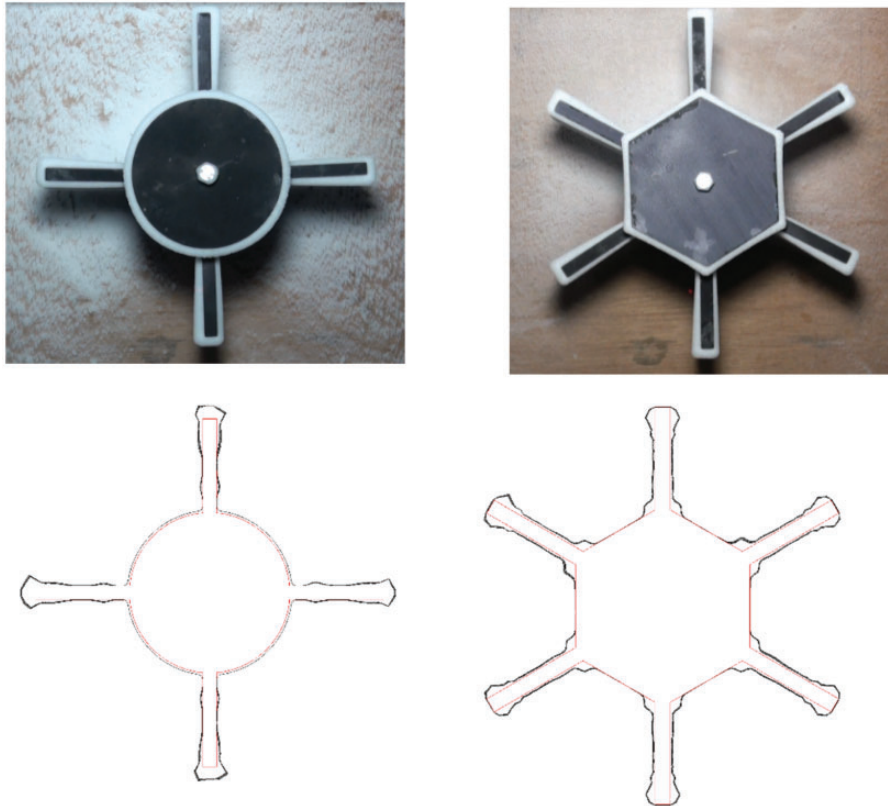


Figure 8. Comparison of accreted ice profile shapes from numerical and experimental analysis for $t = 180$ min.

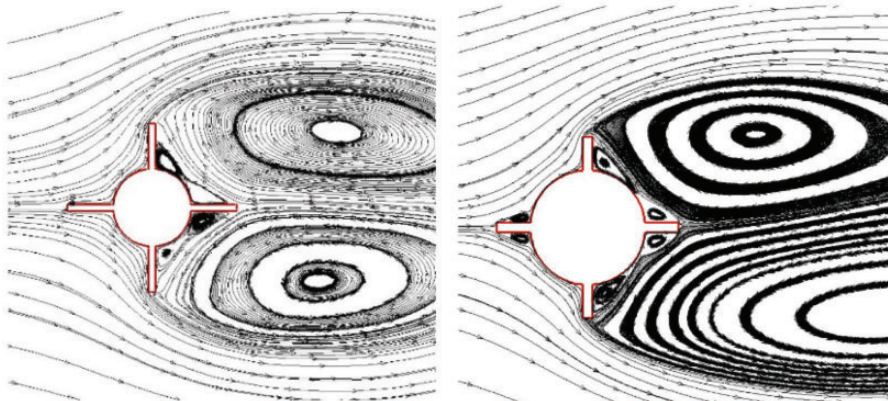


Figure 9. Velocity streamlines for circular cross sections having two different fin sizes (94 and 47 mm).

numerical and experimental analysis for a total duration of 3 h.

Effect of fin length. To understand the effects of fin length on resultant ice growth along rotating geometries, analyses were carried out considering circular cross section at operating conditions specified in Table 1. Two different sizes of fin length (47 and 94 mm) were used for this study. Results show a considerable change in the ice growth with fin size variation. Decrease in fin length

is considerably changing the flow behaviour along the fins, which is resulting in development of stronger flow recirculation zones along the fin section. Figure 9 shows a comparison of velocity streamlines for two different fin size cases.

The change in flow behaviour and development of flow circulation zones along the fins by reducing its size, also affect the droplet behaviour and impingement along surface, which leads to a change in resultant ice accretion. Figure 10 shows the shape of

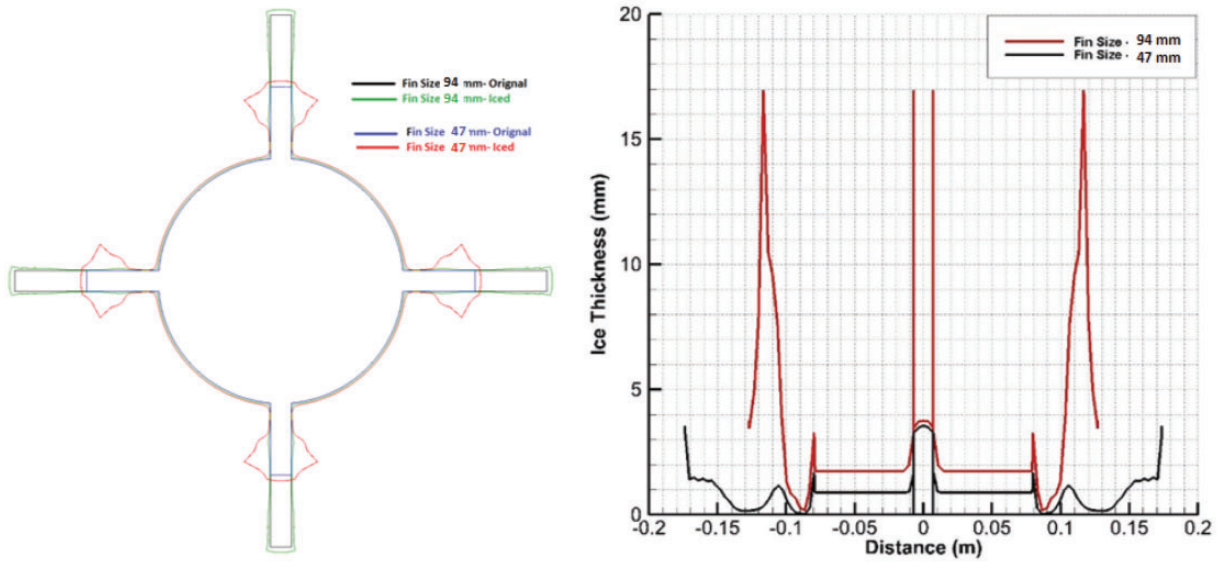


Figure 10. Effect of fin size on ice accretion along the circular cross section.

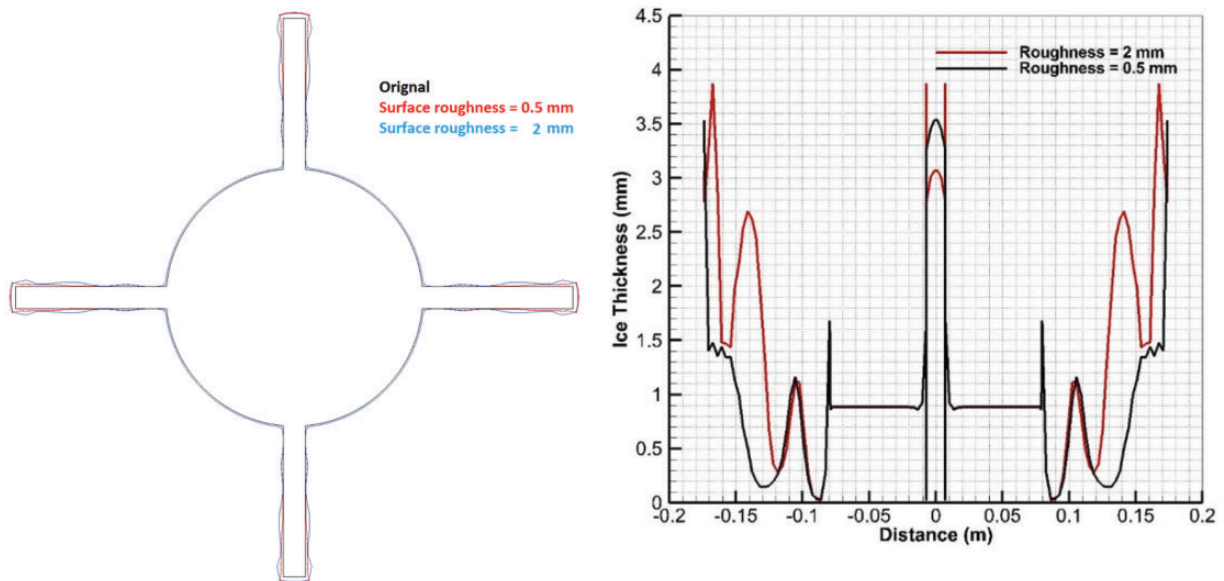


Figure 11. Effect of surface roughness on ice accretion along the circular cross section.

accreted ice and resultant ice thickness for both cases. Analyses show an increase in ice growth particularly along tip sections of fin in case of reducing its length.

Effect of geometric surface roughness. Different geometric surface roughness distributions can result in different ice shapes, due to their influence on water runback characteristics and the resultant ice coverage.²⁶ Along different areas of real iced surface, the roughness should behave as different patterns or texture, according to the

geometric configuration and atmospheric conditions. The surface roughness is known to make an important contribution to the convective heat transfer and surface water mass flow.

The effect of surface roughness on resultant ice growth along the circular cross section has been investigated by imposing two different sand grain roughnesses (0.5 and 2 mm). Figure 11 shows the accumulated ice shapes and ice thickness for two different sand grain roughness along the circular cross section. Analysis shows a considerable change in resultant ice growth

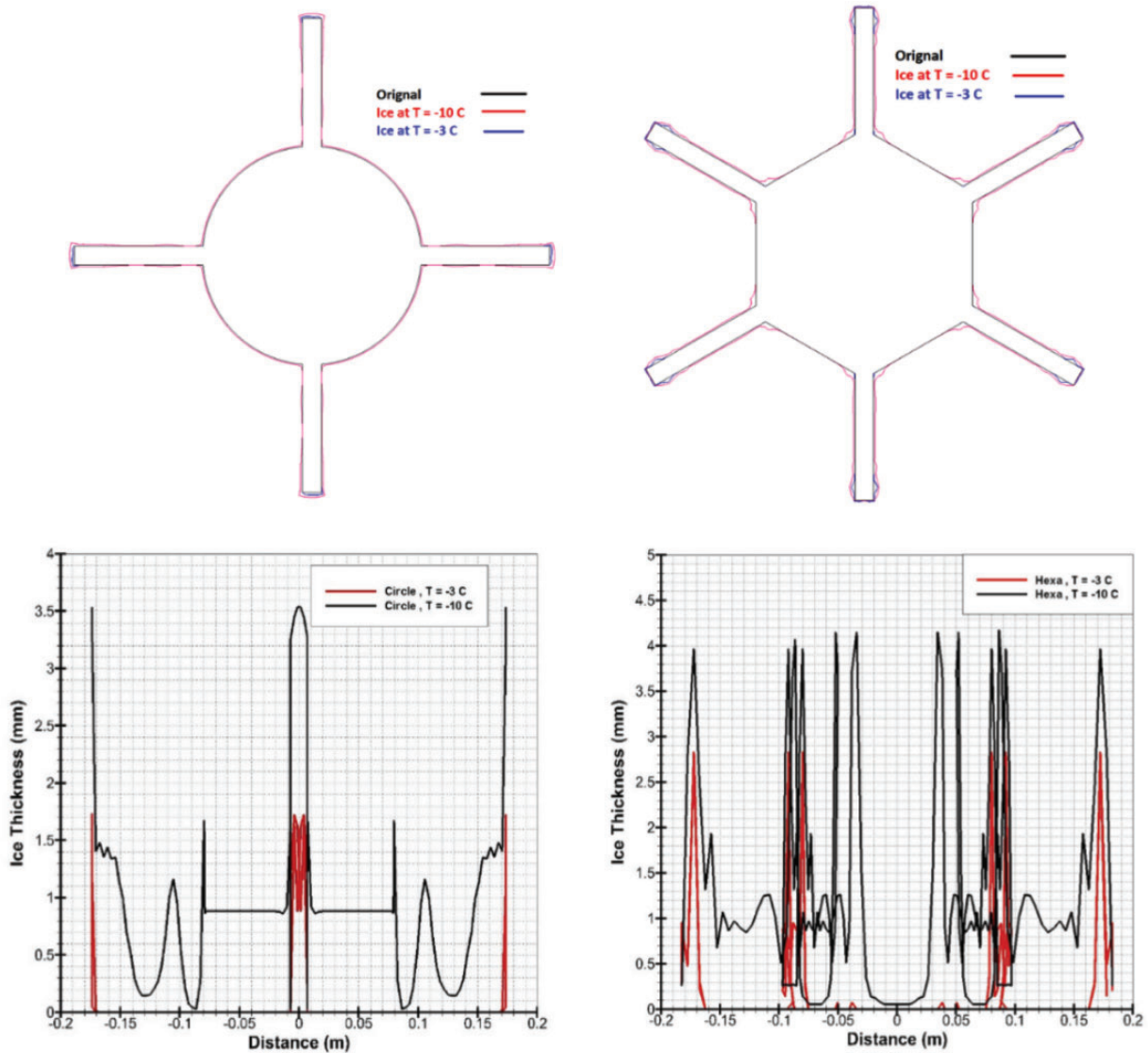


Figure 12. Ice accretion at different atmospheric temperatures for $t = 120$ min.

particularly along fin sections with the increase in surface roughness to 2 mm. Increase in surface roughness increases the possibilities of development of beads along the surface, which possibly leads to an increase in ice accretion. This change in ice accretion is mainly due to change in the tangential and normal shear stress distributions along the surface due to the airflow at the air–water interface that plays a crucial role not only on the convective heat transfer rate at the disturbed air–water interface, but also on the height of the accumulated iced surface roughness.

Study of operating parameters variations

Effects of atmospheric temperature. To study the effects of atmospheric temperature variations on ice accretion, analyses were carried out for both dry and wet ice

conditions ($T = -3$ and -10°C), for circular and hexagonal cross sections. Figure 12 shows the accreted ice shapes and thickness for both geometric cross sections. Results show a significant change in accreted ice shapes for the hexagon with the increase in temperatures, compared with the circular cross sections. At -3°C (for wet ice conditions), more irregular ice shapes were observed near the fin tip sections, but resultant ice growth was less for both geometric cross sections, whereas for the dry rime ice conditions, more regular ice shapes were found with ice growth. The change in accreted ice shape by the variation of atmospheric temperature is somehow also coupled with the flow behaviour, as in the case of hexagon cross section, more disturbed airflow and droplet behaviour is observed, which possibly effects the resultant heat fluxes (aerodynamic and impinging droplet kinetic energy) and shear stress distributions

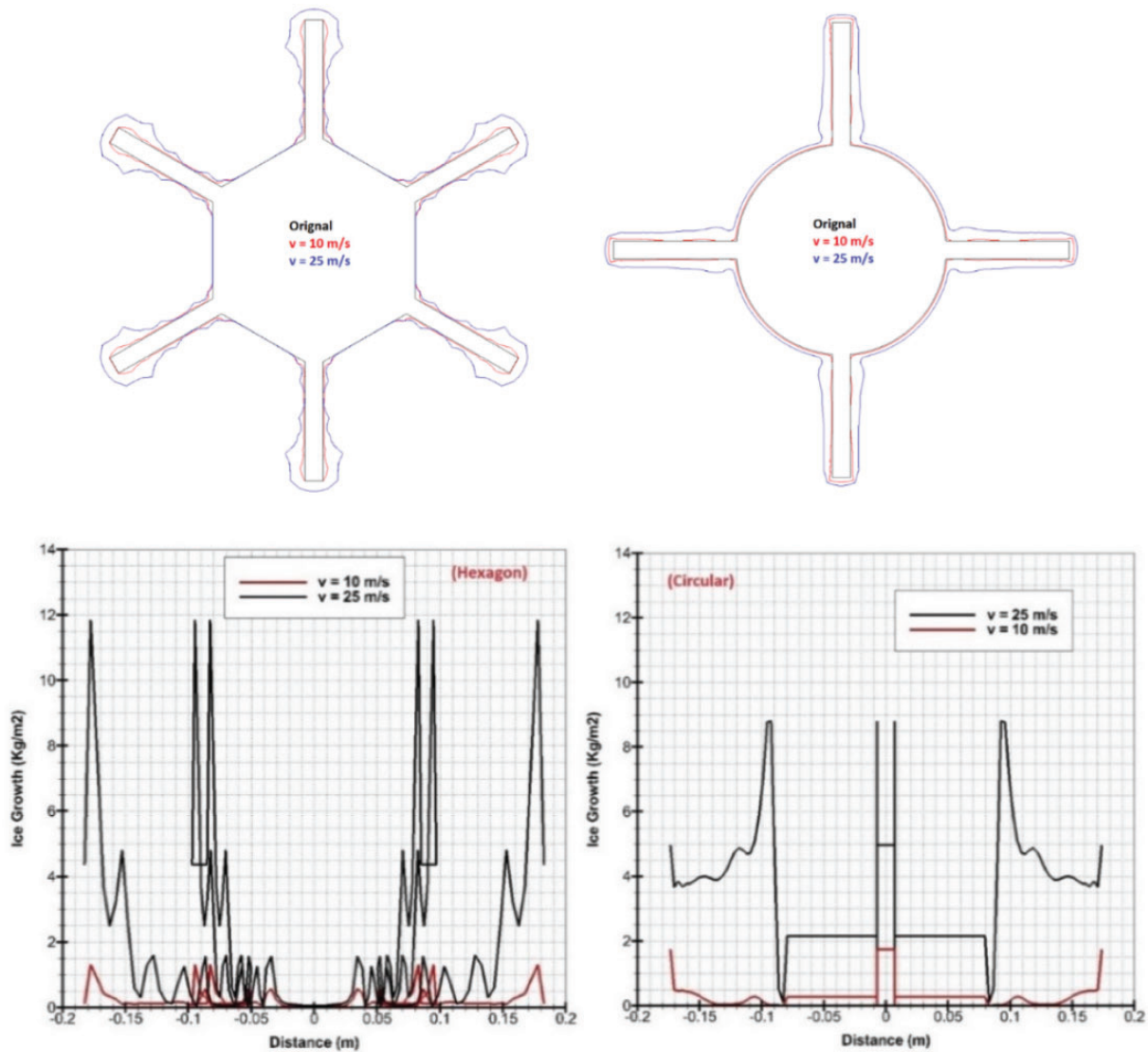


Figure 13. Effect of wind velocity variation on ice accretion, $t = 120$ minutes and $T = -10^\circ\text{C}$.

along the surface that changes the ice growth. The ice growth and thickness in case of hexagon cross section is found to be more irregular at wet ice conditions, compared with the circular cross section.

Effect of wind velocity. To study the effect of wind velocity variations on ice accretion, analyses were carried out at two different wind velocities (10 and 25 m/s) for rotating circular and hexagonal cross sections. Figure 13 shows the accreted ice shapes and growth for both geometries. The analysis shows a significant change in ice growth with the increase of wind velocity for both geometries. An increase in wind velocity increases the possibility of droplet collision with the geometric surface, which results in increase of ice growth. The analysis also shows that in case of hexagon cross section, the ice shapes get more irregular along the fins at high wind

speed, which is mainly due to more irregular flow behaviour along the fins, as discussed above, and also increase in the heat flux due to convection, aerodynamic heating and changes in droplet impingement kinetic energy. Results show that accreted ice shapes in case of circular cross sections remains streamlined compared with hexagonal cross section even at high wind speeds.

Effect of droplets size. To study the effect of water droplet size variation on resultant ice accretion, numerical analyses were carried out for two different droplet sizes ($MVD = 35$ and $70 \mu\text{m}$), at atmospheric air temperature of -10°C and wind speed of 10 m/s. Figure 14 shows the ice growth for two different droplet sizes along the circular cross section. Analysis shows that change in the droplet size effects the ice accretion, as increasing the droplet

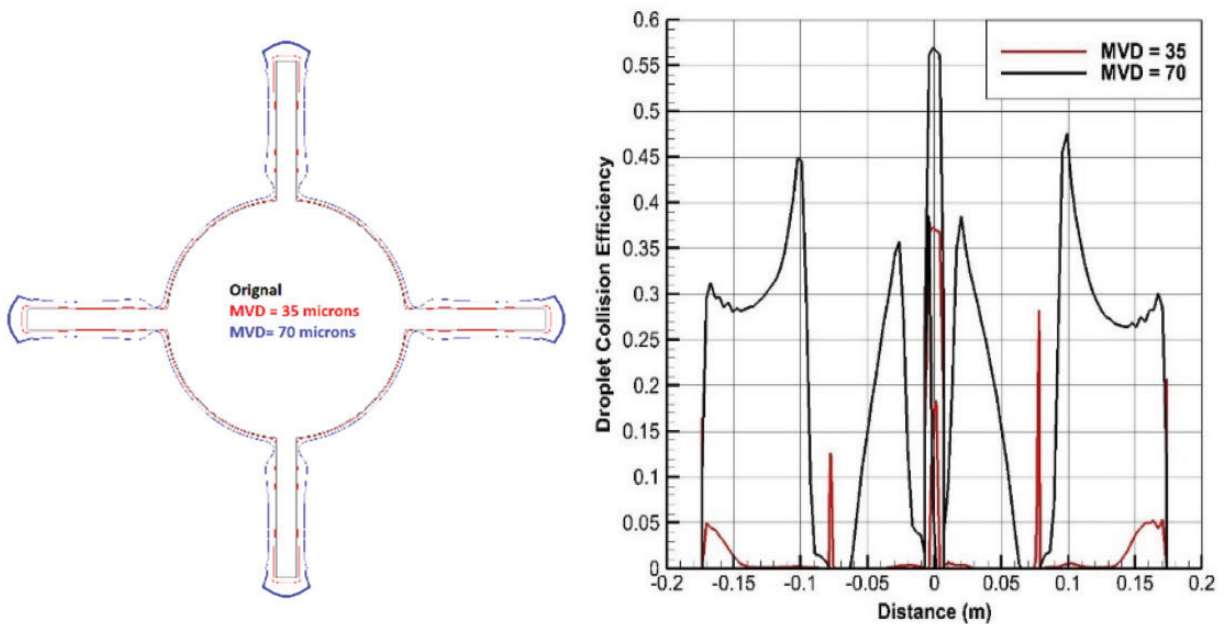


Figure 14. Effect of droplet size variation on ice accretion.

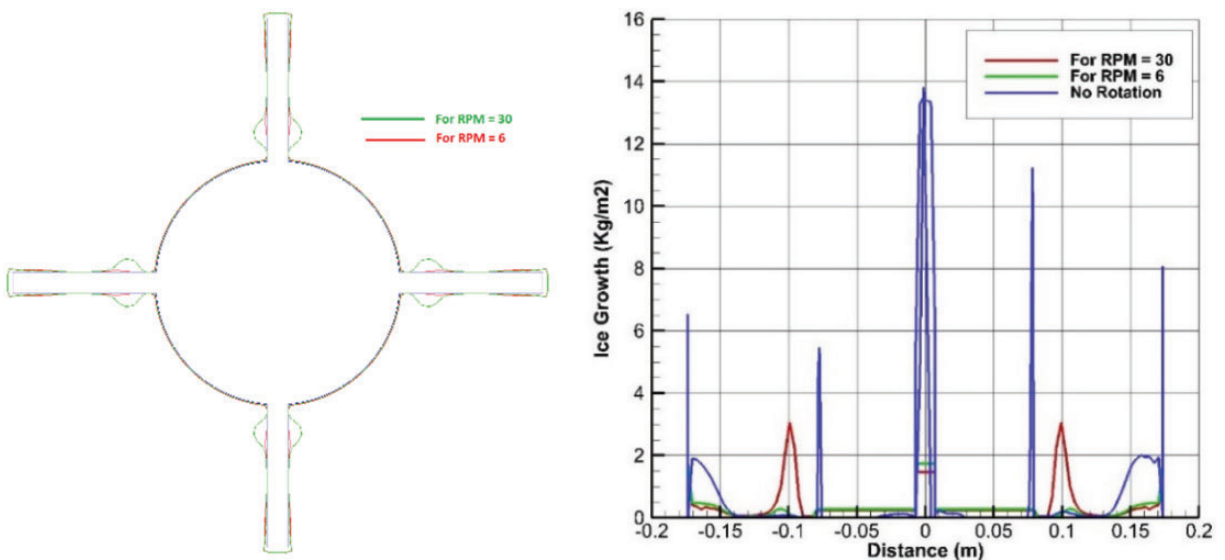


Figure 15. Effect of rotational speed variation on ice accretion.

size increases the possibility of droplet impingement. The main reason for this can also be explained by the fact that larger diameter droplets have larger inertia compared with smaller droplets. Therefore, the movement of larger droplets is less affected by the airflow and more of the droplets collide with the surface, which results in increase of the ice growth.

Effect of rotational speed. To study the effect of geometric rotational speed, numerical analyses carried out for two

different rotational speeds ($r/\text{min} = 6$ and 30) of a circular cross section, at atmospheric air temperature of -10°C and wind speed of 10 m/s . Analysis shows that increase in r/min leads to an increase in ice growth, particularly along the fin sections. This is mainly because increase in the r/min increases the tangential component of flow velocity, which leads to a change in the droplet behaviour and water run back, as results show a development of ice hump near the fin root section.

Conclusion

A CFD-based numerical study has been presented in this paper to understand and analyse the rate and shape of atmospheric ice accretion on three different rotating geometric cross sections having fins. Numerical analyses provided a base to better understand the ice accretion process on each geometric cross section at different operating and geometric conditions. Results showed that overall the ice accretion on circular cross section is smoother and more regular compared with the square and hexagonal cross sections due to more streamlined airflow and droplet behaviour. The result also shows that a fin size of 94 mm at an r/min of 6 with a circular rotating geometry displays a better ice accretion profile shape compared with the hexagonal and square cross sections. The ice accretion profile for the hexagon cross section with six fins was nevertheless better than the square cross section with four fins. This study lays a foundation to select an optimum geometric configuration for rotating component of the newly-designed icing sensor.

Declaration of Conflicting Interests

The author(s) declared no potential conflicts of interest with respect to the research, authorship, and/or publication of this article.

Funding

The author(s) disclosed receipt of the following financial support for the research, authorship, and/or publication of this article: The work reported in this paper was partially funded by the Research Council of Norway, project no. 195153 and WindCoE (Nordic Wind Energy Centre) project funded within Interreg IVA Botnia-Atlantica, as part of European Territorial Cooperation (ETC).

References

1. Myers TG and Charpin JPF. A mathematical model for atmospheric ice accretion and water flow on a cold surface. *Heat Mass Transf* 2004; 47: 5483–5500.
2. Fu P, Farzaneh M and Bouchard G. Two dimensional modelling of the ice accretion process on transmission line wires and conductors. *Cold Region Sci Technol* 2006; 46: 132–146.
3. Cao Y, Zhang Q and Sheridan J. Numerical simulation of ice accretion on airfoils. In: *Proceedings of XXII ICTAM*, Adelaide, Australia, August 2008, pp. 1–2.
4. Wagner T, Peil U and Borri C. Numerical investigation of conductor bundle icing. In: *Proceedings of EACWE 5*, Florence, Italy, July 2009, pp. 473–476.
5. Ackely SF and Templeton MK. *Computer modelling of atmospheric ice accretion*. U.S. Army Cold Region Research and Engineering Laboratory, 36p. Crrel Report No: CR 79-04, 1979.
6. Lozowski EP, Stallabrass JR and Hearty FP. The icing of an unheated, non-rotating cylinder, Part I: a simulation model. *J Climate Appl Meteorol* 1983; 22: 2053–2062.
7. Lozowski EP and Oleskiw MM. *Computer modelling of time dependant rime icing in the atmosphere*. U.S. Army Cold Region Research and Engineering Laboratory, 74p. Crrel Report No: CR 83-02, 1983.
8. Lozowski EP, Finstad KJ and Gates EM. Comments on calculation of the impingement of cloud droplets on a cylinder by finite element method. *J Atmos Sci* 1985; 42: 306–307.
9. McComber P. Numerical simulation of ice accretion on cables. In: *First international workshop on atmospheric icing on structures*, Hanover, Hampshire, 1–3 June 1983.
10. McComber P, Martin R and Morin G. Estimation of combined ice and wind loads on overhead transmission lines. In: *First international workshop on atmospheric icing on structures*, Hanover, Hampshire, 1–3 June 1983.
11. Smoth BW and Barker CP. Icing of cables. In: *First international workshop on atmospheric icing on structures*, Hanover, Hampshire, 1–3 June 1983.
12. Makkonen L. Models for the growth of rime, glaze, icicles and wet snow on structures. *Philos Transact Royal Soc A* 2000; 358: 2913–2939.
13. Makkonen L, Laakso T and Marjaniemi M. Modelling and prevention of ice accretion on wind turbines. *Wind Eng* 2001; 25: 3–21.
14. Finstad KJ, Lozowski EP and Gates EM. A computational investigation of water droplet trajectories. *J Atmos Oceanic Technol* 1988; 5: 160–170.
15. Shin J. Prediction of ice shapes and their effect on airfoil drag. *J Aircraft* 1994; 31: 263–270.
16. Shin J and Bind TH. Experimental and computational ice shapes and resulting drag increase for a NACA 0012 airfoil, 1992, NASA technical memorandum 105743.
17. Boutanios Z. *An Eulerian 3D analysis of water droplets impingement on a Convair-580 nose and cockpit geometry*. Montreal, Canada: Concordia University, 1999.
18. Skelton PLI and Poots G. Snow accretion on overhead line conductors of finite torsional stiffness. *Cold Region Sci Technol* 1991; 19: 301–316.
19. Virk M. Numerical study of atmospheric ice accretion on various geometric cross sections. *Wind Eng* 2011; 35: 607–614.
20. Virk MS, Mughal UN and Polanco G. Effect of atmospheric temperature and droplet size variation on ice accretion of wind turbine blades. *J Wind Eng Industrial Aerodynam* 2010; 98: 724–729.
21. Virk MS. Atmospheric ice accretion on circular overhead powerline conductors installed in tandem arrangement. *Int J Computat Multiphase Flow* 2013; 5: 73–81.
22. <http://www.newmerical.com/index.php/en/software/fensap-ice>.
23. Clift R, Grace JR and Weber ME. *Bubbles, drops and particles*. New York: Academic Press, 1978.
24. Özgen S and Canbik E.M. Ice accretion simulation on multi-element airfoils using extended Messinger model. *Heat Mass Transf* 2009; 45: 305–322.
25. Manual, N.S.U., 2010, NTI.
26. Ozer IA, Baruzzi GS and Reid T. FENSAP-ICE: Numerical prediction of ice roughness evolution and its effects on ice shapes. In: *International conference on aircraft and engine icing and ground deicing*, Chicago, IL, 13–17 June 2011.